photonics

MDPI

Article

High-Q Multiband Narrowband Absorbers Based on Two-Dimensional Graphene Metamaterials

Aijun Zhu [1,2,3], Pengcheng Bu [1], Lei Cheng [3,4,*], Cong Hu [1] and Rabi Mahapatra [5]

1 School of Electronic Engineering and Automation, Guilin University of Electronic Technology, Guilin 541004, China; zbluebird@guet.edu.cn (A.Z.); 21082304003@mails.guet.edu.cn (P.B.); hucong@guet.edu.cn (C.H.)
2 Guangxi Key Laboratory of Automatic Detecting Technology and Instruments, Guilin 541004, China
3 Shanxi Key Laboratory of Advanced Semiconductor Optoelectronic Devices and Integrated Systems, Jincheng 048000, China
4 Jincheng Research Institute of Opto-Mechatronics Industry, Jincheng 048000, China
5 Department of Computer Science and Engineering, Texas A&M University, College Station, TX 77843-3112, USA; rabi@tamu.edu
* Correspondence: chenglei@jcgjd.org.cn

Abstract: In this paper, an absorber with multi-band, tunable, high Q, and high sensitivity, based on terahertz periodic two-dimensional patterned graphene surface plasmon resonance (SPR), is proposed. The absorber consists of a bottom metal film separated by a periodically patterned graphene metamaterial structure and a SiO_2 dielectric layer, where the patterned graphene layer is etched by "+" and "L" shapes and circles. It has simple structural features that can greatly simplify the fabrication process. We have analyzed the optical properties of a graphene surface plasmon perfect metamaterial absorber based on graphene in the terahertz region using the finite-difference method in time domain (FDTD). The results show that the absorber device exhibits three perfect absorption peaks in the terahertz bands of f1 = 1.55 THz, f2 = 4.19 THz, and f3 = 6.92 THz, with absorption rates as high as 98.70%, 99.63%, and 99.42%, respectively. By discussing the effects of parameters such as the geometrical dimensions of patterned graphene metamaterial structure "+" width W1, "L" width W2, circular width R, and the thickness of the dielectric layer on the absorption performance of absorber, as well as investigating the chemical potential and relaxation time of patterned-layer graphene material, it was found that the amplitude of the absorption peaks and the frequency of resonance of absorber devices can be dynamically adjusted. Finally, we simulated the spectra as the surrounding refractive index n varied to better evaluate the sensing performance of the structure, yielding structural sensitivities up to 382 GHz/RIU. Based on this study, we find that the results of our research will open new doors for the use of multi-band, tunable, polarization-independent metamaterial absorbers that are insensitive to large-angle oblique incidence.

Keywords: graphene; surface plasmon resonance; the finite-difference time-domain; metamaterial

check for updates

Citation: Zhu, A.; Bu, P.; Cheng, L.; Hu, C.; Mahapatra, R. High-Q Multiband Narrowband Absorbers Based on Two-Dimensional Graphene Metamaterials. *Photonics* **2024**, *11*, 469. https://doi.org/10.3390/photonics11050469

Received: 24 April 2024
Revised: 13 May 2024
Accepted: 15 May 2024
Published: 16 May 2024

1. Introduction

In recent years, the development of ultrafast laser technology has provided a reliable and stable excitation light source for terahertz pulses, which has led to the rapid development of applied research in terahertz technology. With the gradual deepening of the research, many terahertz functional devices have been designed and prepared, which have attracted a lot of researchers' attention, with the advantages of strong absorption, low thickness, and a lightweight absorber. The key issue in designing metamaterial absorbers is finding conventional materials in nature that can be specially customized according to the needs of the abosrober, and designing reasonable artificial parameters to obtain "new materials" with extraordinary physical properties that are different from the original materials' properties [1–4]. Researches have proposed various metamaterial perfect absorber (MPA)

structures [5–11]. With the formation of the absorber structures, the absorption spectra were also determined, which means that the practical application of the absorbers is still limited. In order to develop dynamically tunable metamaterial absorbers, the selection of absorbing materials is considered as the key to overcoming this problem [12–16]. Graphene is a hexagonal honeycomb lattice composed of carbon atoms and sp2 hybridized orbitals [17–20]. Graphene has many special and excellent properties such as a strong electrical conductivity, excellent mechanical properties, and unique optical properties and thermal properties due to its unique two-dimensional structure. This makes graphene metamaterials some of the most promising materials for designing ultra-narrow-band perfect absorbers [21–24]. Meanwhile, compared with conventional metal surface plasma, graphene surface plasma has the advantages of a large mode confinement, long propagation distance in the infrared region, and transport properties that can be tuned by changing the chemical potential, bias electric field, and temperature [25–27]. When the incident light is infrared and the terahertz bands, graphene, and conventional metals have similar properties, the surface can support SPP propagation as well as surface plasmon resonance (SPR) [28]. Therefore, when graphene is combined with metamaterials, the metamaterials can enhance light absorption by exciting surface plasmon resonance [29]. Most studies have focused on narrowband ideal absorbers with single-peak and double-peak absorption [30,31], but relatively few studies have been conducted on multiband ideal narrowband absorbers. This is due to strict limitations that make it difficult to realize perfect absorbers with a multi-band narrowband with simple absorber structures. In general, narrowband absorption can be achieved using Fabry–Perot resonators, metallic gratings, photonic crystals, plasma metamaterials, and guided-wave resonances, while narrowband absorbers designed by plasma metamaterials are structurally simpler, more feasible to manufacture, and, most importantly, dynamically tunable in frequency using the tunable 2D material graphene [32–35].

In our work, we present a perfect metamaterial absorber based on terahertz periodic tunable plasma. The metamaterial absorber consists of copper, silicon dioxide, and patterned graphene layers, ordered from the bottom to the top. Due to the flexibility of the above structure, we can tune its response to light by changing the structural parameters. Throughout this study, we discussed not only the structural parameters, but also the effects of chemical potential, relaxation time, and incident angle on absorption at different polarizations. Finally, we also explored the sensing properties of this structure. We found that our proposed structure can also be used for sensors and detectors in terahertz.

2. Structure and Theory

As shown in Figure 1, the designed graphene metamaterial array structure consists of three layers: the bottom layer is a metallic copper with a thickness H1 of 0.475 μm, in which the electrical conductivity of copper in the metal loss model is $\sigma = 5.8 \times 10^7$ S/m; the middle layer is a silica (SiO_2) dielectric separator with a thickness h of 4.52 μm, which separates the patterned graphene nanostructured layer of the top layer from the copper layer of the bottom layer. Its relative dielectric constant and effective refractive index are $\varepsilon d = 3.9$ and ns = 1.97, respectively [36]; the top layer consists of graphene metamaterial array structures with the geometrical parameters of L1 = 2.1 μm, W1 = 1.3 μm, L2 = 1.25 μm, W2 = 0.25 μm, g = 0.3 μm, R1 = 2.4 μm, and R2 = 3.0 μm, and the structural period is Px = Py = 6.4 μm. The thickness of the single-layer graphene sheet is 0.34 nm, but in our study, we assumed that the effective medium thickness is $\Delta = 1$ nm, to match the thickness of the three-layer graphene sheet. In the experimental process, an electron beam evaporation technique was used to deposit a Cu thin film and a SiO_2 isolation layer onto a silicon substrate, and then a chemical vapor deposition technique was used to grow a graphene layer on a copper catalyst, which was transferred to a SiO_2 isolation layer using a wet method. Patterned graphene was achieved by electron beam lithography and oxygen plasma etching [37]. Finally, the photoresist was stripped to obtain the final structure.

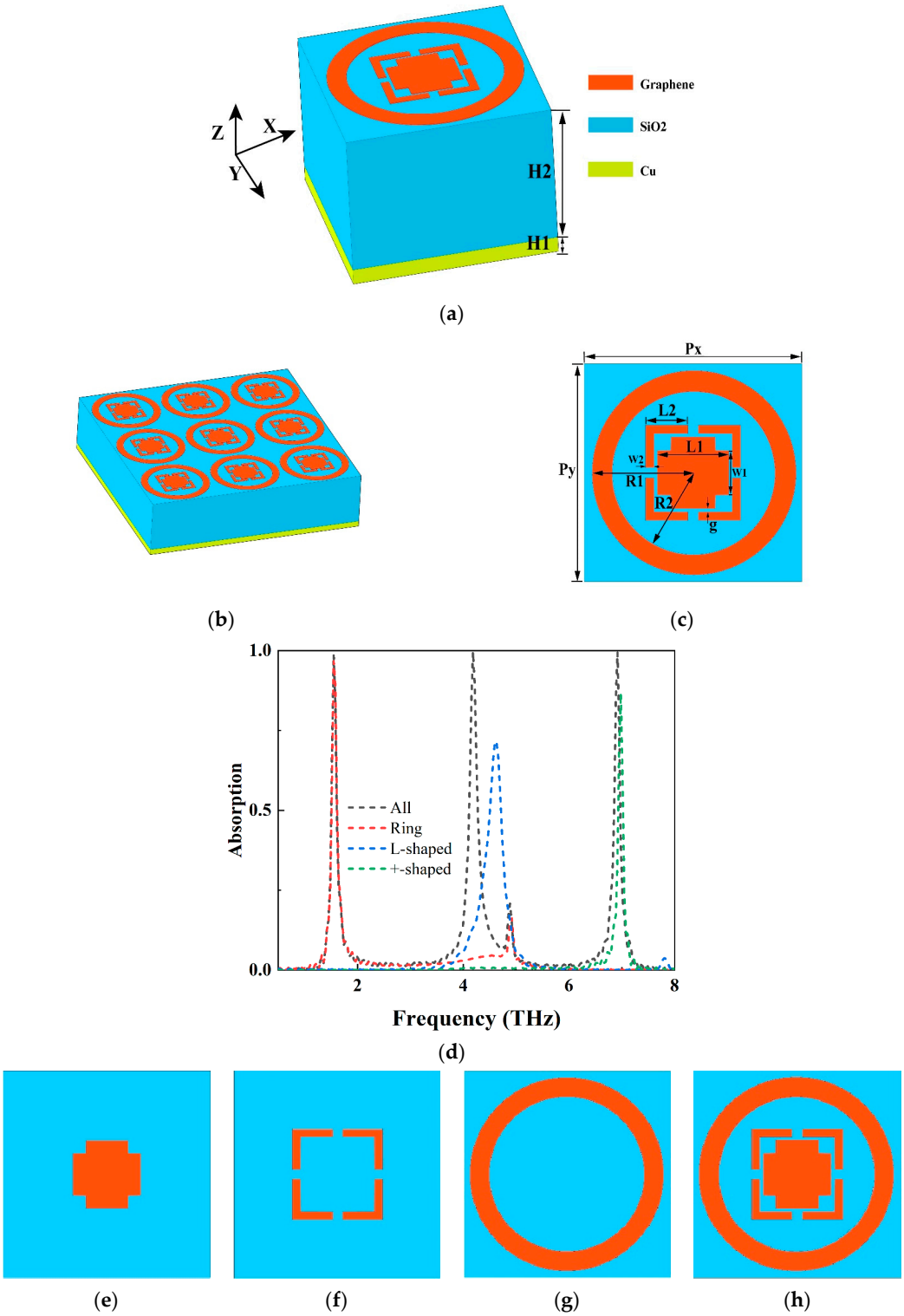

Figure 1. (**a**) Schematic of the unit structure of a tunable perfect absorber based on periodically patterned graphene; (**b**) three-dimensional schematic of the absorber; (**c**) structural diagram of the top layer of graphene; (**d**) absorption spectra of the proposed perfect absorber (black solid line), the structure with only circular graphene arrays (red dashed line), the structure with only "L" shaped graphene arrays (blue dashed line), and the structure with only "+" shaped graphene arrays (green dashed line); (**e**) top view of the "+"-shaped graphene layer's unit structure; (**f**) top view of four "L"-shaped graphene layer's unit structures; (**g**) top view of a circular graphene layer's unit structure; (**h**) top view of a patterned graphene layer's unit structure.

In order to better study the absorption of this absorber, it is first necessary to characterize the optical response of graphene. Since graphene is a two-dimensional material, according to the Kubo formula [38–40], the surface conductivity of graphene can be described as follows:

$$\sigma(\omega, \Gamma, \mu_c, T) = \sigma_{inter}(\omega, \Gamma, \mu_c, T) + \sigma_{intra}(\omega, \Gamma, \mu_c, T) \tag{1}$$

$$\sigma_{inter} = \frac{ie^2}{4\pi\hbar} ln \frac{2|\mu_c| - (\omega + i2\Gamma)\hbar}{2|\mu_c| + (\omega + i2\Gamma)\hbar} \tag{2}$$

$$\sigma_{intra} = \frac{ie^2 k_B T}{\pi\hbar^2(\omega + i2\Gamma)} \left[\frac{\mu_c}{k_B T} + 2In\left(1 + e^{-\frac{\mu_c}{k_B T}}\right) \right] \tag{3}$$

where e is the electron charge, $\hbar$ is the approximate Planck constant, and k_B is the Boltzmann constant. The scattering rate is related to the electron relaxation time (τ) by $2\Gamma = \tau^{-1}$. ω is the angular frequency of the incident wave and μ_c is the graphene chemical potential. As the chemical potential is $|\mu_c| \gg \hbar\omega/2$ in the terahertz and far-infrared bands, the interband contribution to graphene conductivity is negligible according to the principle of bubbly repulsion, and the surface conductivity of graphene is mainly dependent on the in-band contribution. Therefore, σ_{intra} is mathematically solved and converted to the Drude form of the conductivity at room temperature as follows [41–43]:

$$\sigma_g = \frac{ie^2\mu_c}{\pi\hbar^2(\omega + i\tau^{-1})} \tag{4}$$

The dielectric constant of graphene can be obtained from the equation $\varepsilon(\omega) = 1 + i\sigma_g/\omega\varepsilon_0\Delta$ [44], where Δ, ε_0, σ_g, and ω denote the graphene thickness, vacuum permittivity, electrical conductivity, and angular frequency, respectively. Since doped graphene has a negative dielectric constant in the infrared region, which is similar to that of metals in the visible region, strongly confined and long-lived surface plasmon resonance can be supported at the graphene/dielectric interface. In order to obtain the best performance, a simulation and analysis were carried out using FDTD Solutions optical software (version 2020 R2), and the structural parameters were optimized using progressive simulation [45] to obtain the optimal values after comprehensive consideration. In the boundary condition setting, the x/y direction of the cell was defined as a periodic boundary condition, while a perfectly matched layer was used in the Z direction to satisfy the absorption boundary condition [38]. The mesh accuracy was set to dx = dy = 0.4 μm and dz = 0.2 μm, respectively, which is a value that ensures the convergence and reliability of the computational results. In addition, the transmittance T and reflectance R were captured using the frequency-domain field and power monitors. The absorptivity A can be calculated from the equation $A = 1 - T - R$. Since the thickness of the bottom Cu material is much larger than the skinning depth of the electromagnetic wave, the transmittance obtained by the monitor was almost zero. In other words, the absorption efficiency can be expressed as A = 1− R, and complete absorption can be realized when R approaches zero [46,47]. On this basis, we obtained three resonant frequencies corresponding to three strong absorption peaks in the terahertz band—f1 = 1.55 THz, f2 = 4.19 THz, and f3 = 6.92 THz—where the absorption efficiencies for modes A, B, and C are 98.70%, 99.63%, and 99.42%, respectively.

3. Results and Discussion

In order to better understand the principle of narrow-band absorption, we plotted the electric fields used to analyze the three peaks. The surface electric field distributions for f1 = 1.55 THz, f2 = 4.19 THz, and f3 = 6.92 THz were obtained by simulation using the FDTD software (version 2020 R2), as shown in Figure 2a–i. Among them, (a), (b), and (c) in the x-y plane are the electric field distributions at the frequencies of 1.55 THz, 4.19 THz, and 6.92 THz, respectively. Absorption peaks of 1.55 THz are mainly distributed on the left and right sides of the circular structure of the patterned graphene, and 4.19 THz absorption

peaks are mainly concentrated in the "L" shaped patterned graphene and its coupling with the "+" shaped structure. The electric field of the 6.92 THz absorption peak is mainly concentrated in the "+" shaped patterned graphene structure and the left and right sides of the structure, which are stronger than the upper and lower sides. The electric field is stronger on the left and right sides of the "+" shaped patterned graphene structure than on the top and bottom sides. The reason for this distribution is that the coupling between the surface plasma and the electric field of graphene leads to the resonance of electric dipoles, which regionalizes and enhances the electromagnetic field, resulting in a non-uniform distribution of the electric field. According to this explanation, graphene locally absorbs incident light at specific wavelengths and the absorber achieves a peak absorption of more than 98.5% at all three positions.

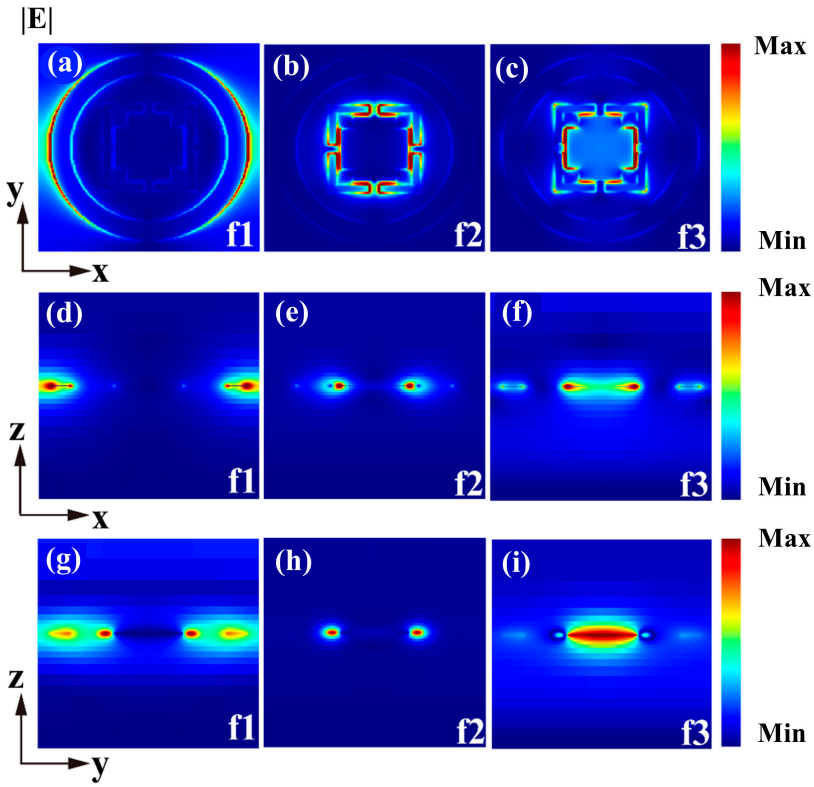

Figure 2. (**a**–**c**) Electric field strength distribution at the top of the absorber in the x-y plane for different resonant frequencies; (**d**–**f**) electric field intensity distribution in the x-z plane at different resonant frequencies; (**g**–**i**) electric field intensity distribution in the y-z plane at different resonant frequencies. The resonant frequencies are f1 = 1.55 THz, f2 = 4.19 THz, and f3 = 6.92 THz.

The resonance mode of the surface plasma can usually be subdivided into two forms. The first is the form of electromagnetic waves propagating at the interface of a metallic medium, called propagating plasma resonance. The second is the electromagnetic wave with energy binding to the closed surface of metal nanoparticles/nanocavities, called localized plasmon resonance (LSPR) [48]. The graphene LSPR has an electric field localization function, which we show in the side view of the electric field at three frequencies in Figure 2d–i. In summary, the electric field collects in the part of the absorber with the graphene pattern, while there is almost no electric field in the part outside the pattern. According to the periodicity condition, the graphene electric field distribution is periodic throughout the absorber. According to the periodicity condition, the distribution of the graphene electric field is periodic throughout the absorber. This ability to locally concentrate the electric field also concentrates the light in the vicinity of the graphene, exactly explaining the perfect absorption achieved by the absorber at three frequencies.

Next, we will further investigate the effect of different factors of the absorber on its absorption rate. The effects of the geometrical parameters of each subpart of the proposed graphene metamaterial structure ("L" shape width, "+" shape dimensions, and circular width) on the absorptive performance of this absorber are analyzed to achieve the optimal structural geometry. As shown in Figure 3, when the proposed graphene metamaterial structure is stabilized in terms of the circular width and "+" shape's length L1 and width W1, with the spacing g, the "L" shape's width W2 varies from 0.20 μm to 0.30 μm, and with the increase in width, the resonance peak frequencies of all three modes show a blue shift, and the absorption efficiency first increases and then decreases. It is shown that the resonant absorption efficiencies of all three modes are maximized at the "L" shape width W2 = 0.25 μm.

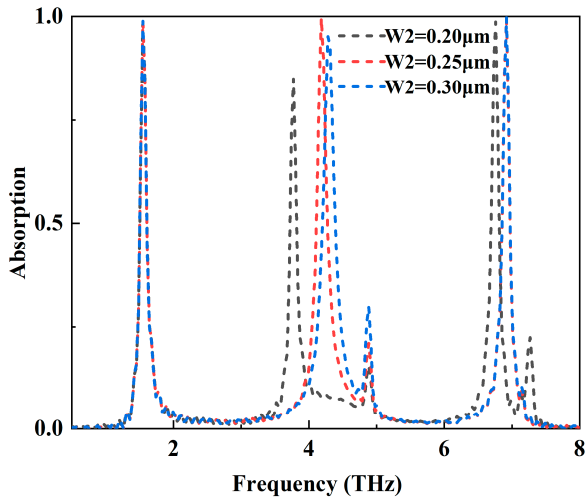

Figure 3. The absorption spectra of fixed, patterned, circular, and "+" shape graphene parameters with the "L" shape's width W2 changing from 0.20 μm to 0.30 μm.

Similarly, as shown in Figure 4, when the proposed absorber structure is stabilized in terms of the circular width, the "L" width W2, and the "+" width W1, the "+" length L1 varies from 1.30 μm to 2.10 μm. With the increase in length, the resonance peak frequencies of the three modes are red-shifted, the absorption efficiency gradually increases, and the absorption peaks of the three modes reach the optimum value at the "+" shape L1 = 2.10 μm. Similarly, we studied the effect of the change in the width W1 of the "+" shaped from 0.1 μm to 2.10 μm on the absorption performance of the proposed absorber, as shown in Figure 5, and the experimental results show that the three modes have the best absorption performance in the case of the "+" shape with the width W1 = 1.30 μm. The experimental results show that the absorption performance of the three modes is the best at the "+" width W1 = 1.30 μm. As shown in Figure 6, when the "L" shape width and "+" shape structure size of the proposed graphene metamaterial structure, as well as the spacing g, are stabilized, the circular width varies from 0.40 μm to 0.80 μm, and the experimental results show that the circular width is 0.60 μm. The experimental results show that the combined absorption performance of the three modes of the absorption peaks is more favorable when the ring width is 0.60 μm. After we adopted the above dimensions for the patterned graphene layer structure size with optimal absorption performance, we investigated the thickness of the dielectric layer SiO_2, as shown in Figure 7, and the experimental results showed that the thickness of the dielectric layer SiO_2, H2, was optimal for the absorption performance at the thickness of H2 = 4.52 μm, when it ranged from 2.02 μm to 7.02 μm. Therefore, optimizing the geometry of the structure is very important to obtain a better absorption performance.

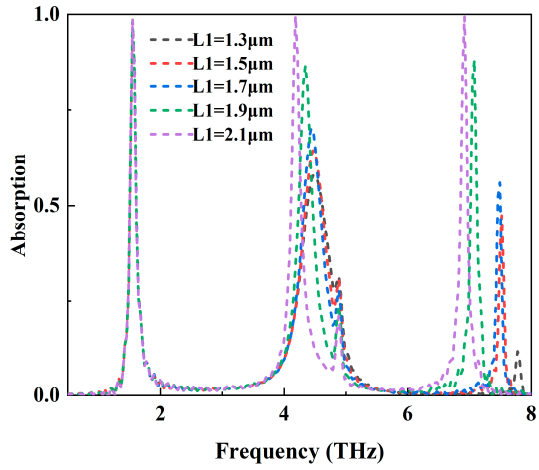

Figure 4. Absorption spectra of the fixed patterned circular and "L" shape graphene parameters with the "+" shape's length L1 changing from 1.3 μm to 2.1 μm.

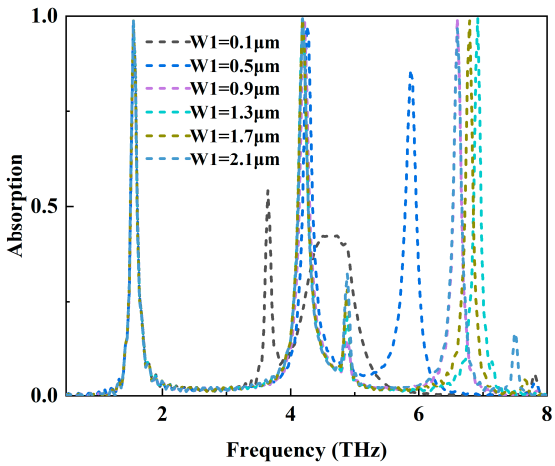

Figure 5. Absorption spectra of fixed patterned rings and "L" shape graphene parameters with "+" shape's width W1 changing from 0.1 μm to 2.1 μm.

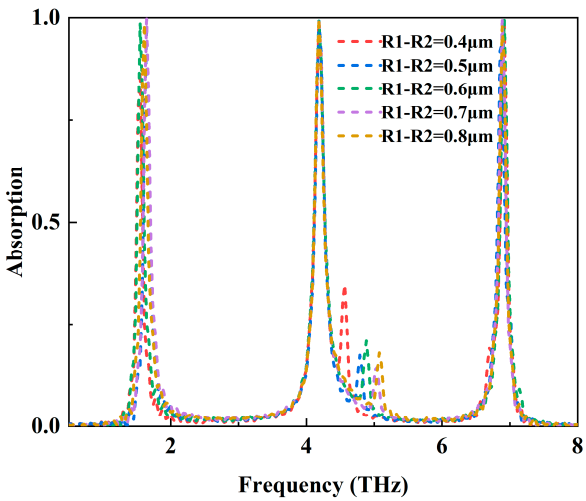

Figure 6. Absorption spectra of the fixed patterned "+" and "L" shape graphene parameters with a change in the width of the rings from 0.4 μm to 0.8 μm.

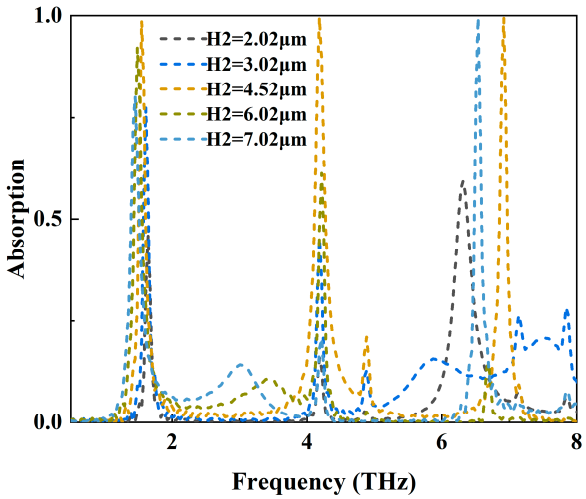

Figure 7. Absorption spectra of the fixed patterned graphene for each parameter, with the thickness of the dielectric layer H2 changing from 2.02 μm to 7.02 μm.

For patterned graphene metamaterial absorbers with fixed structural dimensions, tunability is equally valuable for each application. It is worth noting that the surface conductivity of graphene depends strongly on the chemical potential and the electronic relaxation time. Firstly, we experimentally controlled the chemical potential of patterned graphene layers by applying gate voltage (electrostatic) or chemical doping to study the effect of the chemical potential of graphene layers on the absorption properties of the proposed structures. The corresponding equations are calculated as follows [49–52]:

$$\mu_C = V_f \sqrt{\frac{\pi \varepsilon_0 \varepsilon_r V_g}{e_0 t_d}} \tag{5}$$

where t_d is the thickness of the dielectric layer, V_g is the applied voltage, V_f is the Fermi velocity, e_0 is the charge carried by the electrons, and ε_0 and ε_r denote the vacuum-order permittivity and relative permittivity of the dielectric, respectively. Figure 8 shows the absorption curves by plotting the chemical potential of the patterned graphene from 0.60 eV to 1.40 eV at 0.20 eV intervals under the condition that the light wave is positively incident in the terahertz band. Obviously, the absorption peaks corresponding to the three modes are blueshifted with the increase in graphene chemical potential, and the absorption efficiency first increases and then decreases. The absorption performance of the three modes reaches the optimum when the chemical potential of patterned graphene is 1.0 eV.

We next investigated the effect of the electrons' relaxation time in graphene on the absorption properties of the proposed structure, which is expressed as follows [53,54]:

$$\tau = \mu_c v / \left(e V_f^2 \right) \tag{6}$$

where V_f = 10^6 m/s denotes the Fermi velocity, e = 1.6 × 10^{-19} J/s denotes the electron charge, μ_C denotes the chemical potential, and v denotes the carrier mobility of graphene. In our experiments, we set the chemical potential of the patterned graphene layer at 1.0 eV, and by placing organic molecules on graphene, the carrier mobility of graphene can be significantly increased, thereby controlling the increase in the relaxation time τ [55]. As shown in Figure 9, the absorption efficiencies of the three modes change from 0.50 Ps to 4.00 Ps with the change in the relaxation time τ at a fixed chemical potential μ_C = 1.0 eV.

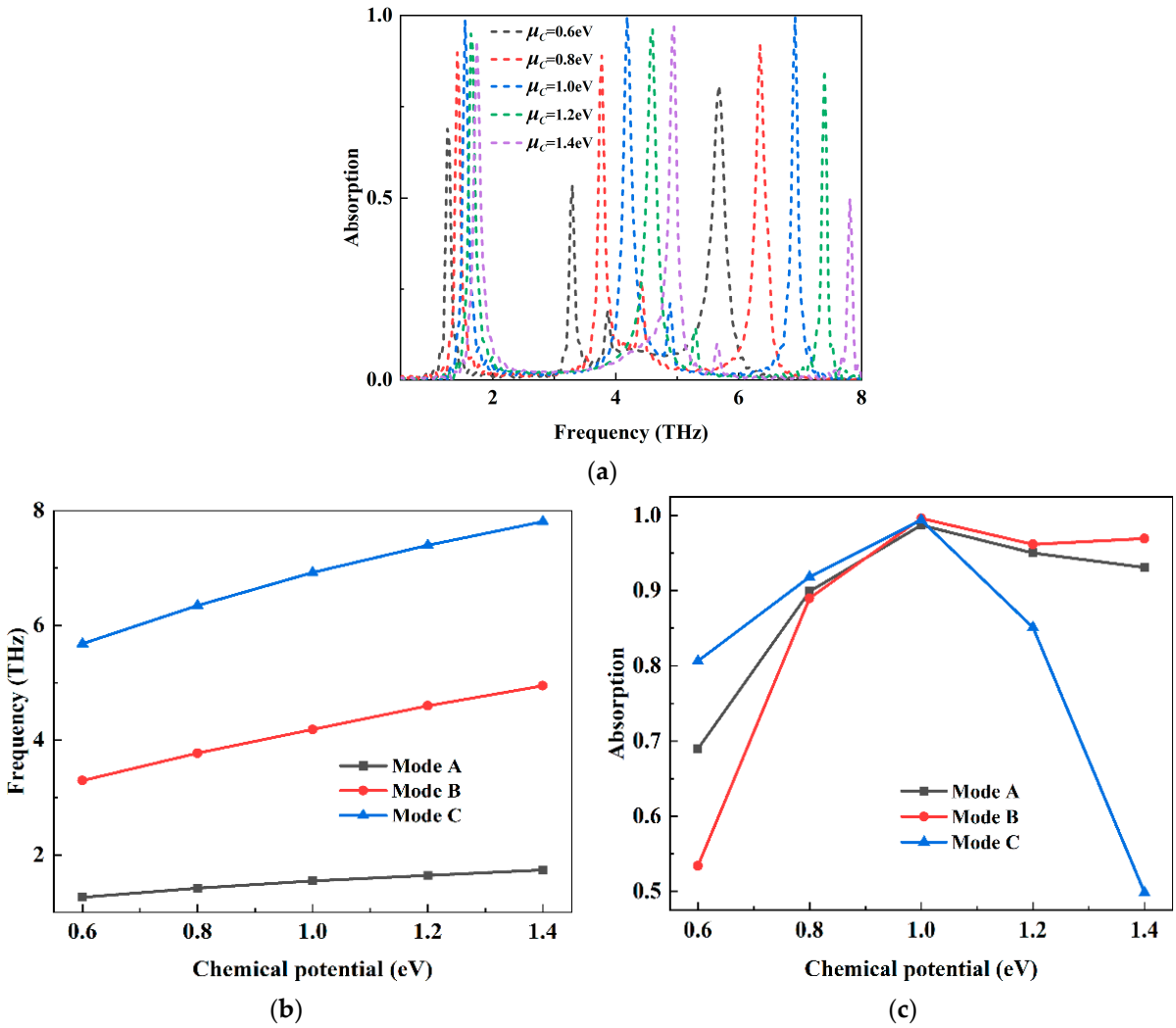

Figure 8. (**a**) Absorption spectra obtained by changing the chemical potential of graphene from 0.6 to 1.4 eV; (**b**,**c**) the resonance frequency and peak absorption intensity spectra of the three modes with the change in chemical potential, respectively.

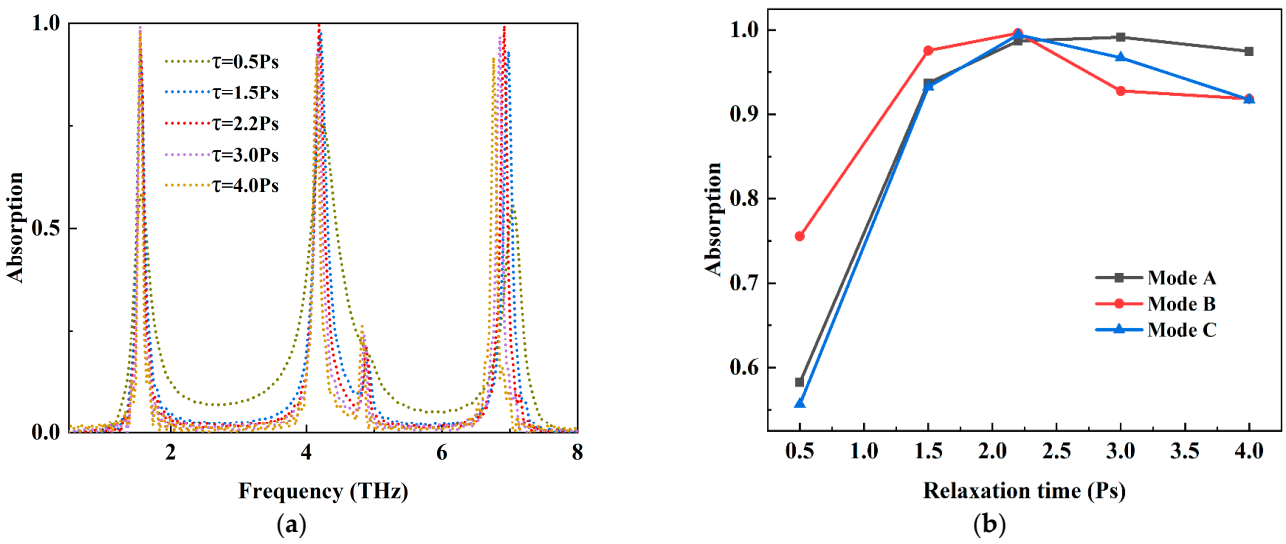

Figure 9. (**a**) Absorption spectra of the absorber for different relaxation times τ. (**b**) Absorption peak versus relaxation time τ for modes A, B, and C.

It is obvious that the position of the absorption peaks is red-shifted with the change in the relaxation time τ, while the peaks of the absorption peaks increase and then decrease, and the bandwidth gradually becomes narrower. Figure 9 shows the variation rule of the absorption peak with relaxation time τ for the three modes. When the relaxation time τ was varied from 0.50 Ps to 4.00 Ps, the adsorption peaks of the three modes ranged from 58.24.% to 99.14% (Mode A), 75.54% to 99.63% (Mode B), and 55.64% to 99.42% (Mode C), respectively. The modulation ranges of the absorption peaks were 41.25%, 24.18%, and 44.04%, respectively. The absorption peaks of the three modes are close to the maximum when μ_C = 1.0 eV and τ = 2.2 Ps. At this point, the carrier concentration of graphene is close to saturation with respect to the plasma oscillations, and a continued increase will result in a decrease in absorption as the relaxation time increases and most of the light is reflected.

For the refractive index sensing properties of the proposed absorber structure, we increased the refractive index of the external environment from 1.0 to 1.5 with a spacing of 0.1. The absorption spectra of the three modes were obtained in turn, as shown in Figure 10, and it can be clearly seen that the resonance frequencies of the three modes were red-shifted as the refractive index n was changed. The redshift of mode A was from 1.548 THz to 1.516 THz, and the redshift of mode B was from 4.186 THz to 4.059 THz. The redshift of mode C was from 6.918 THz to 6.727 THz. The full width at half peaks (*FWHWs*) of the three modes were 0.108 THz, 0.166 THz, and 0.118 THz, respectively. Sensitivity and *FOM* are important parameters for the characterization of important parameters of sensing performance, which can be expressed as follows [56–60]:

$$s = \frac{\Delta T}{\Delta n} \tag{7}$$

$$FOM = \frac{s}{FWHM} \tag{8}$$

$$Q = \frac{f_r}{FWHM} \tag{9}$$

where ΔT denotes the variation in the resonance peak frequency of the absorber with respect to the refractive index Δn of the external environment, and *FWHM* is the full width of the half peak at the absorption peak.

Figure 10a is a plot showing the relationship between the variation in the refractive index with the external environment and the variation in the frequency position of the absorption peak. According to Equation (7), the slope of the fitted straight line is the sensitivity of the proposed graphene metamaterial structure when used as a sensor. The calculated sensitivities of the three modes are 64 GHz/RIU, 254 GHz/RIU, and 382 GHz/RIU, respectively. It can be seen that the three modes of the absorber are sensitive to the change in the resonance frequency of the absorption peaks with respect to the change in the ambient refractive index. In addition, the absorption peaks of the three modes decrease with the increase in the ambient refractive index, but all of them maintain more than 90% perfect absorption, as shown in Figure 10d. Therefore, the high sensitivity of this structure has promising application in the field of sensing and detection. *FOM* can quantify the sensitivity of the sensor. According to Equation (8), the maximum *FOM* of the resonance peaks of the three modes can be calculated as 0.59, 1.53, and 3.24, respectively. After comparison, our absorber has a superior sensitivity and Q, with a dynamic tuning ability, as shown in Table 1 in recent studies [54,61–65].

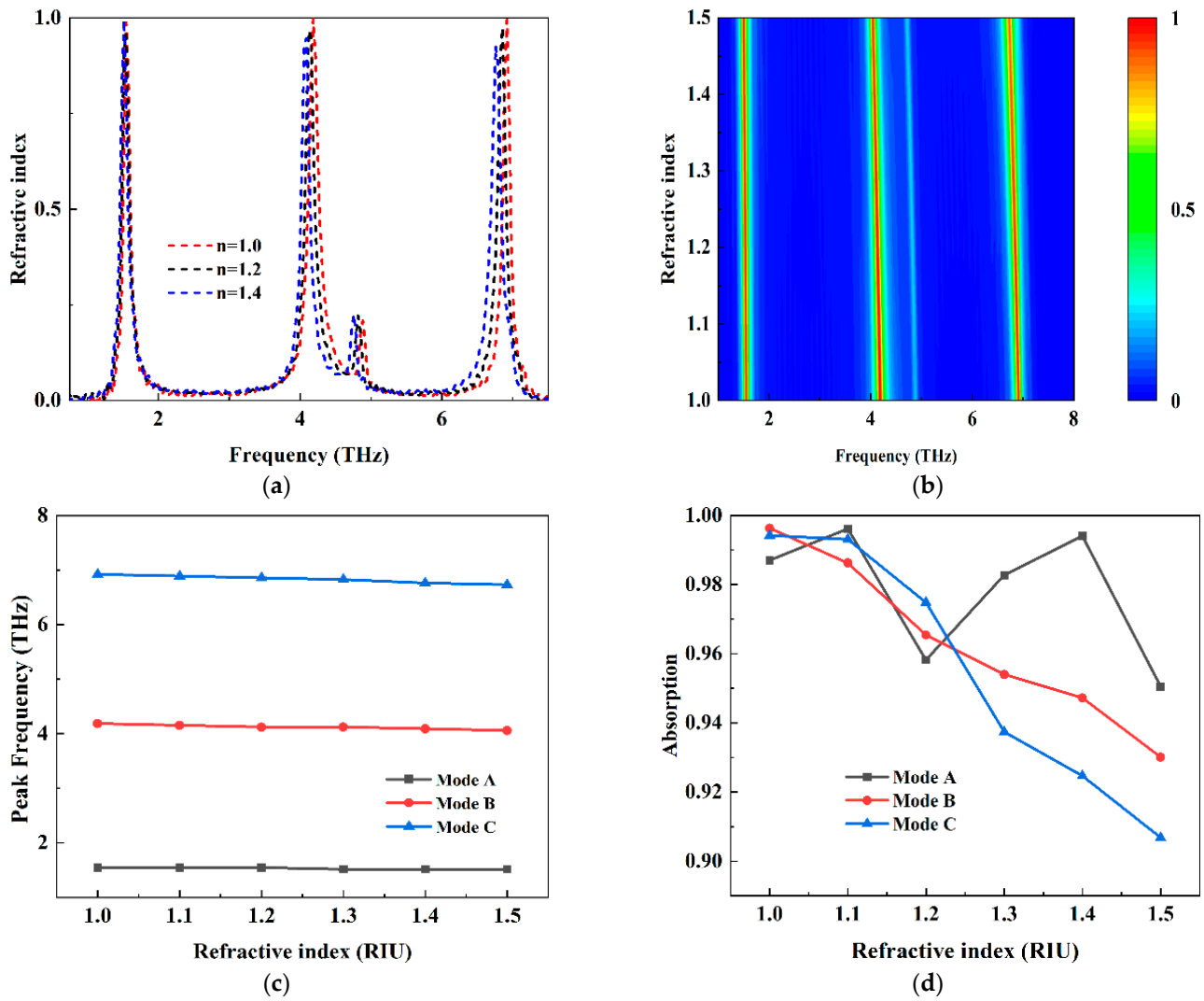

Figure 10. (**a**) Absorption spectra of mode A, mode B, and mode C at different refractive indices; (**b**,**c**) linear relationship between resonant frequency and refractive index; (**d**) linear relationship between absorption peaks and refractive index.

Table 1. Comparison of the proposed absorber with other similar absorbers.

Structure	Sensitivity (RIU^{-1})	*FOM* (Max)	Q	Tunability	Absorption Peak Number	Ref.
Microfiber and $MoTe_2$	590 (nm/RIU)	55	/	No	1	[54]
Graphene and AL_2O_3	282 (nm/RIU)	34.3	/	Yes	1	[61]
Graphene and SIO_2	942.6 (nm/RIU)	/	/	Yes	3	[62]
Graphene and STO	50 (GHz/RIU)	0.33	14	Yes	2	[63]
Graphene and Au	15.0 (um/RIU)	4.19	/	Yes	1	[64]
Graphene and Glass	113.9 (GHz/RIU)	3.15	11.22	Yes	1	[65]
Graphene and Cu	382 (GHz/RIU)	3.24	58.64	Yes	3	This work

It is worth mentioning that the wave absorber proposed in this paper has obvious advantages, such as a simple fabrication and high stability. The results show that our designed sensitivity sensor has a better sensing performance and broader application prospects.

In the above work, the absorption properties of the structure under the positive incidence of terahertz waves were investigated. However, in practical applications, the polarization-independent and angle-of-incidence-insensitive properties of the absorber are also important. Figure 11 shows the effect of polarization angle and incidence angle on

the absorption characteristics of the absorber. Figure 11a shows the relationship between the variation in polarization angle from 0° to 90° and the absorption spectrum for a verical terahertz wave incident, and the results show that the position and intensity of the absorption peaks remain almost constant at vertical incidence due to the good symmetry and local resonance of the absorber. The absorption plots of TE polarization and TM polarization as a function of the frequency and angle of incidence were investigated, as shown in Figure 11b,c. The angle of incidence ranges from 0° to 50°. For TE polarization, the three absorption peaks are almost unaffected, and the absorption remains above 90% when the incident angle is increased from 0° to 50°. The absorption of peak 2 decreases gradually with an incidence angle greater than 50°. For TM polarization, the structure can maintain stable absorption below an incidence angle of 50°, the absorption peaks gradually become bluer, and the absorption bandwidth narrows after the incidence angle becomes larger than 50°. Therefore, we consider this structure to be a polarization-insensitive absorber with a tunable absorption frequency and amplitude.

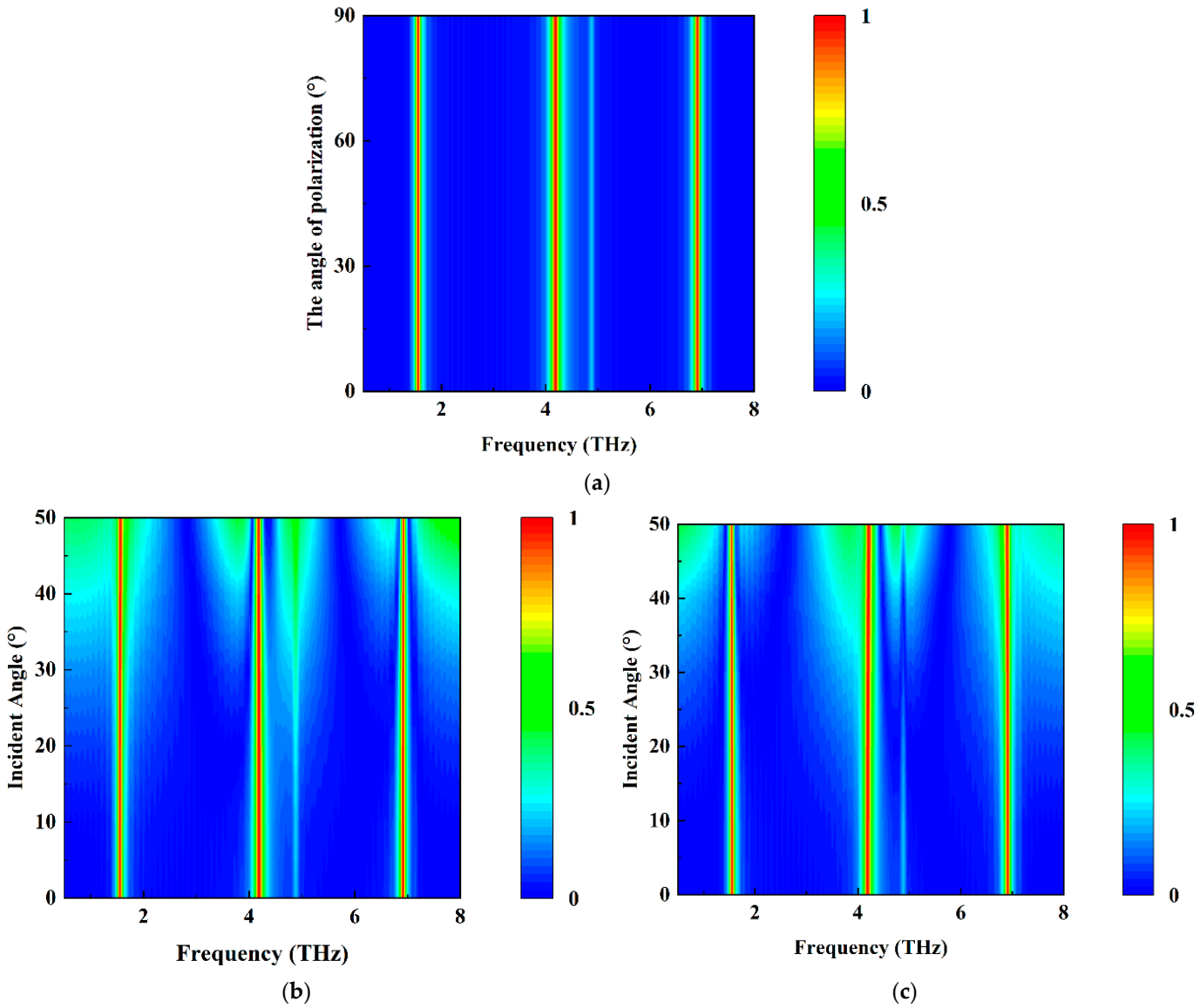

Figure 11. (**a**) Absorption spectra for different polarization angles; (**b**,**c**) the absorption spectra of incident light at angles of incidence ranging from 0°to 50° for TE polarization and TM polarization, respectively.

4. Conclusions

In this paper, a multi-band tunable narrowband absorber with high sensitivity and a high Q based on graphene metamaterial is proposed. The simulation results show that the absorber can obtain three perfect absorption peaks: f1 = 1.55 THz, f2 = 4.19 THz, and f3 = 6.92 THz, with absorption rates of 98.70%, 99.63%, and 99.42%, respectively. The geometrical parameters, chemical potentials, relaxation times, polarization angles, and incidence angles of incident light of the patterned graphene structural units were investigated. It is found that the amplitude of the resonant frequency and amplitude of the absorber unit structure can be flexibly controlled by varying the geometrical parameters and chemical formula of the patterned graphene. By studying and analyzing the variation in the refractive index of the sensing medium, the structure is shown to have a good performance and high-sensitivity response. For modes A, B, and C, the sensitivities are 64 GHz/RIU, 254 GHz/RIU, and 382 GHz/RIU, and the modulation depths are 41.25%, 24.18%, and 44.04%, respectively. In addition, the absorption performance of the absorber remains unchanged as the polarization angle changes, indicating that the absorber is polarization-independent. Based on this, our results will open new doors for the use of multi-band, tunable, polarization-independent, and insensitive-to-large-angle oblique incidence metamaterial absorbers. In the future, they can be applied in the fields of photoelectric detection, photovoltaic cells, photoelectric sensors, and photoelectric thermal radiation.

Author Contributions: Conceptualization and model, A.Z.; numerical simulation, A.Z. and P.B.; writing—original draft preparation, A.Z. and P.B.; investigation and formal analysis C.H.; writing—review and editing, A.Z., P.B. and L.C.; project administration and resources, R.M. All authors have read and agreed to the published version of the manuscript.

Funding: This work is partially funded by the National Natural Science Foundation of China (62161008, 62341116), the Guangxi Natural Science Foundation Joint Funding Project (2018GXNSFAA138115), Guangxi Key Laboratory of Automatic Detecting Technology and Instruments (YQ22110), the Open Project Program of Shanxi Key Laboratory of Advanced Semiconductor Optoelectronic Devices and Integrated Systems (No. 2023SZKF04, No. 2023SZKF10), Shanxi Province Science and Technology Major Program (No. 202201030201009).

Institutional Review Board Statement: Not applicable.

Informed Consent Statement: Not applicable.

Data Availability Statement: The data supporting the findings of this study are available within the article.

Conflicts of Interest: The authors declare no conflicts of interest.

References

1. Pendry, J.B.; Holden, A.J.; Robbins, D.J.; Stewart, W.J. Magnetism from conductors and enhanced nonlinear phenomena. *IEEE Trans. Microw. Theory Tech.* **1999**, *47*, 2075–2084. [CrossRef]
2. Shelby, R.A.; Smith, D.R.; Schultz, S. Experimental verification of a negative index of refraction. *Science* **2001**, *292*, 77–79. [CrossRef]
3. Smith, D.R.; Padilla, W.J.; Vier, D.C.; Nemat-Nasser, S.C.; Schultz, S. Composite medium with simultaneously negative permeability and permittivity. *Phys. Rev. Lett.* **2000**, *84*, 4184–4187. [CrossRef]
4. Yawen, Z.; Limei, Q.; Chang, L.; Junsheng, Y.; Zhijiao, C.; Xiaoming, L.; Yuan, Y.; Xiaodong, C. Investigation of asymmetric transmission devices based on metamaterials. *Chin. J. Quantum Electron.* **2018**, *35*, 385–394.
5. Cai, Y.; Wang, Z.; Yan, S.; Ye, L.; Zhu, J. Ultraviolet absorption band engineering of graphene by integrated plasmonic structures. *Opt. Mater. Express* **2018**, *8*, 3295–3306. [CrossRef]
6. Huang, X.; Yang, F.; Gao, B.; Yang, Q.; Wu, J.; He, W. Metamaterial absorber with independently tunable amplitude and frequency in the terahertz regime. *Opt. Express* **2019**, *27*, 25902–25911. [CrossRef] [PubMed]
7. Liao, Y.-L.; Zhao, Y. Ultra-narrowband dielectric metamaterial absorber for sensing based on cavity-coupled phase resonance. *Results Phys.* **2020**, *17*, 103072. [CrossRef]
8. Meng, W.W.; Lv, J.; Zhang, L.; Que, L.; Zhou, Y.; Jiang, Y. An ultra-broadband and polarization-independent metamaterial absorber with bandwidth of 3.7 THz. *Opt. Commun.* **2019**, *431*, 255–260. [CrossRef]
9. Wu, T.; Wang, G.; Jia, Y.; Shao, Y.; Gao, Y.; Gao, Y. Dynamic modulation of THz absorption frequency, bandwidth, and amplitude via strontium titanate and graphene. *Nanomaterials* **2022**, *12*, 1353. [CrossRef]

10. Yan, Z.; Lu, X.; Chen, K.; Lv, Z.; Pu, X.; Tang, C.; Cai, P. Ultranarrow Dual-Band Perfect Absorption in Visible and Near-infrared Regimes Based on Three-Dimensional Metamaterials for Ultrahigh-Sensitivity Sensing. *J. Light. Technol.* **2021**, *39*, 7217–7222. [CrossRef]
11. Ye, L.; Chen, X.; Zhuo, J.; Han, F.; Liu, Q.H. Actively tunable broadband terahertz absorption using periodically square-patterned graphene. *Appl. Phys. Express* **2018**, *11*, 102201. [CrossRef]
12. Kocer, H.; Butun, S.; Aydin, K.; Banar, B.; Wang, K.; Wu, J.; Tongay, S. Thermal tuning of infrared resonant absorbers based on hybrid gold-VO_2 nanostructures. *Appl. Phys. Lett.* **2015**, *106*, 161104. [CrossRef]
13. Schalch, J.; Duan, G.; Zhao, X.; Zhang, X.; Averitt, R.D. Terahertz metamaterial perfect absorber with continuously tunable air spacer layer. *Appl. Phys. Lett.* **2018**, *113*, 061113. [CrossRef]
14. Song, Z.; Wang, K.; Li, J.; Liu, Q.H. Broadband tunable terahertz absorber based on vanadium dioxide metamaterials. *Opt. Express* **2018**, *26*, 7148–7154. [CrossRef] [PubMed]
15. Ye, L.; Chen, Y.; Cai, G.; Liu, N.; Zhu, J.; Song, Z.; Liu, Q.H. Broadband absorber with periodically sinusoidally-patterned graphene layer in terahertz range. *Opt. Express* **2017**, *25*, 11223–11232. [CrossRef] [PubMed]
16. Zhao, X.; Wang, Y.; Schalch, J.; Duan, G.; Cremin, K.; Zhang, J.; Chen, C.; Averitt, R.D.; Zhang, X. Optically modulated Ultra-Broadband All-Silicon metamaterial Terahertz absorbers. *ACS Photonics* **2019**, *6*, 830–837. [CrossRef]
17. Cen, C.; Zhang, Y.; Chen, X.; Yang, H.; Yi, Z.; Yao, W.; Tang, Y.; Yi, Y.; Wang, J.; Wu, P. A dual-band metamaterial absorber for graphene surface plasmon resonance at terahertz frequency. *Phys. E Low-Dimens. Syst. Nanostruct.* **2020**, *117*, 113840. [CrossRef]
18. Liu, H.; Liu, X.; Zhao, F.; Liu, Y.; Liu, L.; Wang, L.; Geng, C.; Huang, P. Preparation of a hydrophilic and antibacterial dual function ultrafiltration membrane with quaternized graphene oxide as a modifier. *J. Colloid Interface Sci.* **2020**, *562*, 182–192. [CrossRef]
19. Wang, P.; Yao, T.; Li, Z.; Wei, W.; Xie, Q.; Duan, W.; Han, H. A superhydrophobic/electrothermal synergistically anti-icing strategy based on graphene composite. *Compos. Sci. Technol.* **2020**, *198*, 108307. [CrossRef]
20. Zhu, X.; Lin, F.; Zhang, Z.; Chen, X.; Huang, H.; Wang, D.; Tang, J.; Fang, X.; Fang, D.; Ho, J.C.; et al. Enhancing Performance of a GaAs/AlGaAs/GaAs Nanowire Photodetector Based on the Two-Dimensional Electron-Hole Tube Structure. *Nano Lett.* **2020**, *20*, 2654–2659. [CrossRef]
21. He, Z.; Li, L.; Ma, H.; Pu, L.; Xu, H.; Yi, Z.; Cao, X.; Cui, W. Graphene-based metasurface sensing applications in terahertz band. *Results Phys.* **2021**, *21*, 103795. [CrossRef]
22. Liu, Q.; Jiang, Y.; Sun, Y.; Hu, C.; Sun, J.; Liu, C.; Lv, J.; Zhao, J.; Yi, Z.; Chu, P.K. Surface plasmon resonance sensor based on U-shaped photonic quasi-crystal fiber. *Appl. Opt.* **2021**, *60*, 1761–1766. [CrossRef] [PubMed]
23. Liu, W.; Pang, L.; Han, H.; Liu, M.; Lei, M.; Fang, S.; Teng, H.; Wei, Z. Tungsten disulfide saturable absorbers for 67 fs mode-locked erbium-doped fiber lasers. *Opt. Express* **2017**, *25*, 2950–2959. [CrossRef] [PubMed]
24. Zhang, X.; Liu, Z.; Zhang, Z.; Gao, E.; Luo, X.; Zhou, F.; Li, H.; Yi, Z. Polarization-sensitive triple plasmon-induced transparency with synchronous and asynchronous switching based on monolayer graphene metamaterials. *Opt. Express* **2020**, *28*, 36771–36783. [CrossRef] [PubMed]
25. Gao, E.; Liu, Z.; Li, H.; Xu, H.; Zhang, Z.; Luo, X.; Xiong, C.; Liu, C.; Zhang, B.; Zhou, F. Dynamically tunable dual plasmon-induced transparency and absorption based on a single-layer patterned graphene metamaterial. *Opt. Express* **2019**, *27*, 13884–13894. [CrossRef] [PubMed]
26. Qi, Y.; Zhang, Y.; Liu, C.; Zhang, T.; Zhang, B.; Wang, L.; Deng, X.; Bai, Y.; Wang, X. A tunable terahertz metamaterial absorber composed of elliptical ring graphene arrays with refractive index sensing application. *Results Phys.* **2020**, *16*, 103012. [CrossRef]
27. Wang, Y.; Li, R.; Sun, X.; Xian, T.; Yi, Z.; Yang, H. Photocatalytic application of Ag-Decorated CuS/$BaTiO_3$ composite photocatalysts for degrading RhB. *J. Electron. Mater.* **2021**, *50*, 2674–2686. [CrossRef]
28. Liu, L.; Chen, J.; Zhou, Z.; Yi, Z.; Ye, X. Tunable absorption enhancement in electric split-ring resonators-shaped graphene arrays. *Mater. Res. Express* **2018**, *5*, 045802. [CrossRef]
29. Fu, J.; Lv, B.; Li, R.; Ma, R.; Chen, W.; Wang, Z. Excitation of surface plasmon polaritons in an inhomogeneous graphene-covered grating. *Plasmonics* **2017**, *12*, 209–213. [CrossRef]
30. Wang, J.; Song, C.; Hang, J.; Hu, Z.-D.; Zhang, F. Tunable Fano resonance based on grating-coupled and graphene-based Otto configuration. *Opt. Express* **2017**, *25*, 23880–23892. [CrossRef]
31. Wu, P.; Zhang, C.; Tang, Y.; Liu, B.; Lv, L. A perfect absorber based on similar Fabry-Perot Four-Band in the visible range. *Nanomaterials* **2020**, *10*, 488. [CrossRef] [PubMed]
32. Cheng, Z.; Cheng, Y. A multi-functional polarization convertor based on chiral metamaterial for terahertz waves. *Opt. Commun.* **2019**, *435*, 178–182. [CrossRef]
33. Liu, W.; Pang, L.; Han, H.; Shen, Z.; Lei, M.; Teng, H.; Wei, Z. Dark solitons in WS_2 erbium-doped fiber lasers. *Photon. Res.* **2016**, *4*, 111–114. [CrossRef]
34. Wu, P.; Wang, Y.; Yi, Z.; Huang, Z.; Xu, Z.; Jiang, P. A Near-Infrared Multi-Band perfect absorber based on 1D Gold grating Fabry-Perot structure. *IEEE Access* **2020**, *8*, 72742–72748. [CrossRef]
35. Wu, Y.; Wang, X.; Wen, X.; Zhu, J.; Bai, X.; Jia, T.; Yang, H.; Zhang, L.; Qi, Y. Surface-enhanced Raman scattering based on hybrid surface plasmon excited by Au nanodisk and Au film coupling structure. *Phys. Lett. A* **2020**, *384*, 126544. [CrossRef]

36. Jiang, L.; Yuan, C.; Li, Z.; Su, J.; Yi, Z.; Yao, W.; Wu, P.; Liu, Z.; Cheng, S.; Pan, M. Multi-band and high-sensitivity perfect absorber based on monolayer graphene metamaterial. *Diam. Relat. Mater.* **2021**, *111*, 108227. [CrossRef]
37. Nasari, H.; Abrishamian, M.S. Electrically tunable, plasmon resonance enhanced, terahertz third harmonic generation via graphene. *RSC Adv.* **2016**, *6*, 50190–50200. [CrossRef]
38. Yuan, C.; Yang, R.; Wang, J.; Tian, J. Tunable enhanced bandwidth all-graphene -dielectric terahertz metamaterial absorber/reflector. *Optik* **2020**, *224*, 165517. [CrossRef]
39. Zhu, A.; Bu, P.; Cheng, L.; Hu, C.; Mahapatra, R. High-Sensitivity Sensor Based on Diametrical Graphene Strip Plasma-Induced Transparency. *Photonics* **2023**, *10*, 830. [CrossRef]
40. Zhu, A.; Bu, P.; Hu, C.; Niu, J.; Mahapatra, R. High Extinction Ratio 4 × 2 Encoder Based on Electro-Optical Graphene Plasma Structure. *Photonics* **2023**, *10*, 216. [CrossRef]
41. An, S.; Lv, J.; Yi, Z.; Liu, C.; Yang, L.; Wang, F.; Liu, Q.; Su, W.; Li, X.; Sun, T.; et al. Ultra-short and dual-core photonic crystal fiber polarization splitter composed of metal and gallium arsenide. *Optik* **2021**, *226*, 165779. [CrossRef]
42. Qin, F.; Chen, X.; Yi, Z.; Yao, W.; Yang, H.; Tang, Y.; Yi, Y.; Li, H.; Yi, Y. Ultra-broadband and wide-angle perfect solar absorber based on TiN nanodisk and Ti thin film structure. *Sol. Energy Mater. Sol. Cells* **2020**, *211*, 110535. [CrossRef]
43. Zhao, F.; Chen, X.; Yi, Z.; Qin, F.; Tang, Y.; Yao, W.; Zhou, Z.; Yi, Y. Study on the solar energy absorption of hybrid solar cells with trapezoid-pyramidal structure based PEDOT:PSS/c-Ge. *Sol. Energy* **2020**, *204*, 635–643. [CrossRef]
44. Wang, L.; Li, W.; Jiang, X. Tunable control of electromagnetically induced transparency analogue in a compact graphene-based waveguide. *Opt. Lett.* **2015**, *40*, 2325–2328. [CrossRef]
45. You, B.; Zhang, R.; Wang, S.; Han, K.; Shen, X.; Wang, W. A high-performance broadband terahertz absorber based on single layer cross-shaped graphene. *Optik* **2021**, *241*, 167249. [CrossRef]
46. Liu, C.; Wang, J.; Wang, F.; Su, W.; Yang, L.; Lv, J.; Fu, G.; Li, X.; Liu, Q.; Sun, T.; et al. Surface plasmon resonance (SPR) infrared sensor based on D-shape photonic crystal fibers with ITO coatings. *Opt. Commun.* **2020**, *464*, 125496. [CrossRef]
47. Yan, P.; Chen, H.; Liu, A.; Li, K.; Ruan, S.; Ding, J.; Qiu, X.; Guo, T. Self-Starting Mode-Locking by Fiber-Integrated WS_2 Saturable Absorber Mirror. *IEEE J. Sel. Top. Quantum Electron.* **2017**, *23*, 33–38. [CrossRef]
48. Wang, D.; Yi, Z.; Ma, G.; Dai, B.; Yang, J.; Zhang, J.; Yu, Y.; Liu, C.; Wu, X.; Bian, Q. Two-channel photonic crystal fiber based on surface plasmon resonance for magnetic field and temperature dual-parameter sensing. *Phys. Chem. Chem. Phys.* **2022**, *24*, 21233–21241. [CrossRef]
49. Liu, C.; Wang, J.; Jin, X.; Wang, F.; Yang, L.; Lv, J.; Fu, G.; Li, X.; Liu, Q.; Sun, T.; et al. Near-infrared surface plasmon resonance sensor based on photonic crystal fiber with big open rings. *Optik* **2020**, *207*, 164466. [CrossRef]
50. Liu, Y.; Liu, H.; Jin, Y.; Zhu, L. Ultra-broadband perfect absorber utilizing a multi-size rectangular structure in the UV-MIR range. *Results Phys.* **2020**, *18*, 103336. [CrossRef]
51. Luo, H.; Li, Q.; Du, K.; Xu, Z.; Zhu, H.; Liu, D.; Cai, L.; Ghosh, P.; Qiu, M. An ultra-thin colored textile with simultaneous solar and passive heating abilities. *Nano Energy* **2019**, *65*, 103998. [CrossRef]
52. Yang, M.; Jin, L.; He, M.; Yi, Z.; Duan, T.; Yao, W. SiO_x@C composites obtained by facile synthesis as anodes for lithium- and potassium-ion batteries with excellent electrochemical performance. *Appl. Surf. Sci.* **2021**, *542*, 148712. [CrossRef]
53. Tung, N.T.; Phuc, L.H. Lithographic fabrication and spectroscopic characterization of a THz metamaterial absorber. *Vietnam J. Sci. Technol.* **2021**, *59*, 40–46. [CrossRef]
54. Wang, J.; Jiang, Z.; Chen, H.; Li, J.; Yin, J.; Wang, J.; He, T.; Yan, P.; Ruan, S. High energy soliton pulse generation by a magnetron-sputtering-deposition-grown $MoTe_2$ saturable absorber. *Photon. Res.* **2018**, *6*, 535–541. [CrossRef]
55. He, Z.; Xue, W.; Cui, W.; Li, C.; Li, Z.; Pu, L.; Feng, J.; Xiao, X.; Wang, X.; Li, G. Tunable Fano Resonance and Enhanced Sensing in a Simple Au/TiO_2 Hybrid Metasurface. *Nanomaterials* **2020**, *10*, 687. [CrossRef]
56. Rastgordani, A.; Kashani, Z.G. High-sensitive refractive index sensors based on graphene ring metasurface. *Opt. Commun.* **2020**, *474*, 126164. [CrossRef]
57. Sadeghi, Z.; Shirkani, H. Highly sensitive mid-infrared SPR biosensor for a wide range of biomolecules and biological cells based on graphene-gold grating. *Phys. E Low-Dimens. Syst. Nanostruct.* **2020**, *119*, 114005. [CrossRef]
58. Zhu, A.; Li, Z.; Cheng, L.; Hu, C.; Mahapatra, R.N. An Amplitude Tunable Dual-Band Bandpass Filter With Perfect Absorption and Its Sensing Applications. *IEEE Sens. J.* **2024**, *24*, 4387–4399. [CrossRef]
59. Zhu, A.; Li, Z.; Hou, W.; Cheng, L.; Hu, C.; Zhao, T.; Xu, C.; Mahapatra, R. Double plasmon-induced transparency 3 bit graphene encoder. *Diam. Relat. Mater.* **2024**, *142*, 110800. [CrossRef]
60. Zhu, A.; Li, Z.; Hou, W.; Yang, X.; Cheng, L.; Hu, C.; Qiao, F.; Mahapatra, R. A 2-bit graphene encoder based on the plasmon-induced transparency effect and its sensing characteristics. *Results Phys.* **2024**, *59*, 107608. [CrossRef]
61. Safaei, A.; Chandra, S.; Leuenberger, M.N.; Chanda, D. Wide angle dynamically tunable enhanced infrared absorption on Large-Area nanopatterned graphene. *ACS Nano* **2019**, *13*, 421–428. [CrossRef]
62. Wang, L.; Yi, Y.; Yi, Z.; Bian, L.; Zhang, J.; Yang, H.; Chen, J.; Wu, P.; Li, H.; Tang, C. A perfect absorber of multi-band, tunable monolayer patterned graphene based on surface plasmon resonance. *Diam. Relat. Mater.* **2022**, *130*, 109498. [CrossRef]
63. Feng, H.; Zhang, Z.; Wang, J.; Zhang, J.; Fang, D.; Liu, C.; Wang, G.; Gao, Y.; Gao, Y. Individually frequency and amplitude tunable metamaterial absorber with sensing functions based on strontium titanate and graphene. *Diam. Relat. Mater.* **2022**, *130*, 109455. [CrossRef]

64. Yi, Z.; Chen, J.; Cen, C.; Chen, X.; Zhou, Z.; Tang, Y.; Ye, X.; Xiao, S.; Luo, W.; Wu, P. Tunable Graphene-based plasmonic perfect metamaterial absorber in the THz region. *Micromachines* **2019**, *10*, 194. [CrossRef]
65. Almawgani, A.H.M.; Surve, J.; Parmar, T.; Armghan, A.; Aliqab, K.; Ali, G.A.; Patel, S.K. A graphene-metasurface-inspired optical sensor for the heavy metals detection for efficient and rapid water treatment. *Photonics* **2023**, *10*, 56. [CrossRef]